Environ Model Assess (2011) 16:153–167
DOI 10.1007/s10666-010-9241-3

# A Method for Ensemble Wildland Fire Simulation

**Mark A. Finney · Isaac C. Grenfell · Charles W. McHugh · Robert C. Seli · Diane Trethewey · Richard D. Stratton · Stuart Brittain**

Received: 19 January 2010 / Accepted: 5 October 2010 / Published online: 6 November 2010


**Abstract** An ensemble simulation system that accounts for uncertainty in long-range weather conditions and two-dimensional wildland fire spread is described. Fuel moisture is expressed based on the energy release component, a US fire danger rating index, and its variation throughout the fire season is modeled using time series analysis of historical weather data. This analysis is used to characterize the seasonal trend in ERC, autocorrelation of residuals, and daily standard deviation and stochastically generate artificial time series of afternoon fuel moisture. Daily wind speed and direction are sampled stochastically from joint probabilities of historical wind speed and direction for the date range of the fire simulation period. Hundreds or thousands of fire growth simulations are then performed using the synthetic fire weather sequences. The performance of these methods is evaluated in terms of the number of ensemble member simulations, one- versus two-dimensional fire spread simulations, and comparison with results from 91 fires occurring from 2007 to 2009. Simulations were found to be in consistent agreement with observations, but trends indicate that the ensemble average of simulated fire sizes were consistently larger than actual fires whereas the farthest extent burned by fires was underestimated.

M. A. Finney (✉) · I. C. Grenfell · C. W. McHugh · R. C. Seli · D. Trethewey
USDA Forest Service, Rocky Mountain Research Station,
Missoula Fire Sciences Laboratory,
5775 Highway 10 West,
Missoula, MT 59808, USA
e-mail: mfinney@fs.fed.us

R. D. Stratton · S. Brittain
Systems for Environmental Management,
P.O. Box 8868, Missoula, MT 59801, USA

**Keywords** Wildland fire · Fire simulation · Decision support · Fire behavior · Risk assessment

## 1 Introduction

Large wildland fires in the western USA can burn for weeks or months—well beyond the range of weather forecasts routinely used to inform fire spread predictions. Planning and risk assessments for fires over these time frames have, thus, relied on fire projections for a small subset of possible weather scenarios (e.g., [41]). The uncertainty inherent in medium- or long-range predictions of both weather and consequent fire spread suggests the use of ensemble forecasts, similar to those produced by meteorological modeling, to characterize the likely impacts of these long-burning fires and to make risk-informed strategic management decisions. Ensemble forecasts in meteorology, as described by Silvillo et al. [45], can be compiled from the suite of outputs arising from the nonlinear feedback responses of models to variations in the initial conditions (e.g., [46]) or assembled from the results of different models. Operational wildland fire modeling systems (e.g., [6, 20, 39]) lack feedback processes but offer the opportunity for producing ensemble estimates of fire spread based on varying weather scenarios as independent inputs.

The use of ensemble fire behavior calculations is relatively uncommon in fire science and wildland fire management operations. Ensemble fire growth simulations have recently been explored by Anderson et al. [3] where short-term weather parameters were subjected to random variation. Boychuk et al. [10] demonstrated a fire growth simulation with stochastically varied fire behavior. Perhaps the most widely recognized effort to date was a method

proposed by Wiitala and Carlton [48] for estimating fire spread probabilities along a one-dimensional (1D) transect from a point on the current fire edge to a remote point of interest. Their method modeled probabilities as the result of a race between two kinds of stochastic processes—those producing fire movement and those bringing about the end of the fire season [28]. For practical reasons, Wiitala and Carlton [48] simplified their analysis of historical fire weather by categorizing the resulting daily fire behavior events as either "rare and significant" or "common." Rare events were assumed to occur as a Poisson process and produce greater fire spread than common events. Several assumptions of this method had strong influence on the outcome but were necessary given the computing limitations at the time. These include assumptions that (1) fire travel in the direction of interest can be approximated by 1D spread (i.e., along a linear transect), (2) the average spread rate along the transect due to rare and common events can be represented as a harmonic mean (per [26]), (3) fire weather events occur at random, and (4) the sequential order of weather events and fuel types encountered is irrelevant.

The need for many of the assumptions made by Wiitala and Carlton [48] has been obviated by improved computing and availability of weather data, digital fuel and vegetation maps, and enhanced methods for fire growth modeling. The applicability of two-dimensional (2D) fire growth modeling has been widely applied to individual fires over spatially complex terrain for specific sequences of weather (e.g., [ 18, 20, 36]). Current methods of fire growth computation most commonly rely on perimeter expansion (Huygens' principle) or various cell- or node-based algorithms (Fermat's principle) [5]. Each of these techniques can reproduce the basic empirical fire shapes observed under simple conditions, such as ellipses, and respond realistically to spatially and temporally varying environmental conditions [21, 37]. Fire growth models require a spatial grid of fuels and topography used for fire behavior calculations, and these data are now readily available for the USA, from the LANDFIRE Project (http://www.landfire.gov). For practical reasons, weather information is often supplied nonspatially—as a point source or uniform domain of time-varying temporal changes—although the fire growth simulations can ingest spatial data if available.

In the past decade, fire growth simulation has been used increasingly for fire risk assessment. The focus of much of this work has been on estimating burn probabilities for an entire landscape given the uncertainty of ignition locations [1, 12, 31, 34]. Combined with values or resources, the burn probabilities and the distribution of different fire behaviors that cause various effects can be used for risk analysis and estimate expected impacts of wildland fires [17, 23, 43]. Similar risk analyses can be conducted if ensemble calculations were made for individual fires. In this paper, we focus on simulations of a single fire event with a known location and extent. We describe a new approach to producing ensemble fire simulations from a practical set of model and data components. The simulations are intended for evaluating risk associated with a large fire over multiple weeks in an operational environment where the greatest uncertainty is future weather.

## 2 Methods

The goal of this work was to produce an ensemble fire simulation that accounted for uncertainty in fire impact related to weather for a single ignition or fire. A system was envisioned that would generate a large sample of possible weather sequences and run a fire growth simulation for each one. The ensemble would then be summarized by spatial probability fields representing the chance of burning and the variability in fire behavior such as fire intensity.

To accomplish this, we relied on the assumption of Wiitala and Carlton [48] that environmental parameters can be simplified to daily values yet still provide details sufficient for generating fire behavior for the period of the day when active fire spread occurs. It has long been understood that wildland fires are most active, meaning most area is burned, during the afternoon hours or "burning period" compared with nighttime or morning hours when humidity and fuel moisture are higher [8, 13]. A daily value of fire spread is consistent in resolution with the intention of estimating burn probabilities (of fire spread over many days or weeks), given the uncertainty associated with weather conditions over the range of possible fire seasons. Daily afternoon values of fuel moisture are the cornerstone of the National Fire Danger Rating system (NFDRS) [11, 19] expressly because of their demonstrated relevance to potential worst-case fire behavior. Moisture contents of fuel particles from four dead and two live time lag categories are used in fire behavior calculations associated with the NFDRS. The NFDRS produces an index called energy release component (ERC) that reflects only moisture effects on the rate of flaming combustion [11, 19] and has been shown to be strongly related to fire activity [7]. Large woody fuels have longer time lags or characteristic time periods required to asymptotically approach equilibrium moisture contents provided steady conditions [25]. This means that a given day's fuel moisture values are not independent of the previous days' conditions and will be autocorrelated for at least as long as one time lag of the largest woody fuel component. These temporal dependencies have been represented in various ways, including a Markov process [29].

## 3 Weather Generation

We selected a time series approach for analyzing and generating weather sequences because it was able to capture (1) the autocorrelation in daily values of fuel moisture percentages through the proxy ERC index, (2) the seasonal trends throughout a given year, and (3) the variation among seasons. For the purposes of time series modeling and subsequent fire growth simulation, we obtained a sample of daily values of ERC (designated as $z(t)$ and $t$ represents days) from a number of years (e.g., 10 to 20 years). This analysis requires the following assumptions:

1. There exists an overall seasonal trend $f(t)$ which remains the same from year to year, which we estimate with a weighted least squares polynomial model of $z(t)$. The weights were the inverse of the daily standard deviations.
2. Daily standard deviations are estimated assuming $z(t)$ is normally distributed around the daily means $\mu(t)$.
3. The residuals $(z(t)-f(t))$ are autocorrelated in time out to a maximum value of $t^*$ and follow some autocorrelation function $\rho(k)$ where $k$ is the lag in days.

The autocorrelation function $\rho(k)$ is used to obtain coefficients $\varphi$ (for use later in an autoregressive function) as follows:

$$\phi = \mathbf{P}_{t^*}^{-1}\rho_{t^*} \tag{1}$$

where $\phi=[\phi_1, \phi_2,..., \phi_t^*]$ and $\rho_t^*=[\rho_1, \rho_2,..., \rho_t^*]$and the matrix $P=$

$$\begin{array}{cccc} 1 & \rho_1 & \rho_2 & \cdots & \rho_{t^*-1} \\ \rho_1 & 1 & \rho_1 & \cdots & \rho_{t^*-2} \\ \cdots & \cdots & \cdots & \cdots & \cdots \\ \rho_{t^*-1} & \rho_{t^*-2} & \rho_{t^*-3} & \cdots & 1 \end{array}$$

The overall model for estimating autocorrelated time series values of ERC is then:

$$zhat(t) = f(t) + \phi_1(a(t-1)) + \phi_2(a(t-2)) + \ldots + \phi_t^*(a(t-t^*)) + a(t) \tag{2}$$

In this expression, $a(t)$ is a white noise process with zero mean and a variance obtained from Box and Jenkins ([9], p. 56) which accounts for the variance explained by the autoregressive model:

$$\sigma^2(t) = \mathrm{var}(a(t))/(1-\rho_1\phi_1-\rho_2\phi_2\ldots-\rho_t^*\phi_t^*) \tag{3}$$

For the purpose of simulating artificial time series ERC values, we then simulate a stream of artificial $a(t)$'s with $\mathrm{var}(a(t)) = s^2(t)^*(1-\rho_1\phi_1-\rho_2\phi_2\ldots-\rho_t^*\phi_t^*)$. With that stream in hand, we apply the filter $\varphi$ and add the seasonal trend as per Eq. 2.

Given an initial series of ERC values that represent observations up to the day $k$ of the calculations $z(1)$, ... $z(k)$ (bold line in Fig. 1a), we can simulate the remainder of a season using the coefficients obtained in Eq. 3, along with the daily standard deviations $\sigma(t)$ and the trend function $f(t)$ by first simulating $z(k+1)$ using $z(k)$, ... , $z(k-p)$ in Eq. 3. This generates possible ERC time series that reflect the recorded variation in potential ERC trends for the specified number of days beyond the last observation (Fig. 1a).

The season-end date is defined by the threshold ERC value $z^*$ as the minimum value of ERC under which fires will burn. Season end occurs at $z^*$ if ERC does not later exceed that value (e.g., under conditions of renewed drying and warming after rains in late autumn). The season-end date is identified by decrementing in time from the end of the simulated year until the first instance where the value of $z$ exceeds $z^*$. The distribution of season ending event dates for a given threshold ERC can be summarized in cumulative form as the probability of season end by a particular date (Fig. 1b).

The daily ERC values generated by the time series modeling were translated into representative fuel moisture percentages using a look-up table of historical fuel moistures associated with ERC ranges by percentile category (Table 1). The length of time for which these moistures were to apply during the afternoon "burning period" for daily fire spread calculations was then determined from expert judgment (Table 1). In practice, the burning period set for simulation could be adjusted by a local fire behavior analyst.

Wind speed and direction for fire behavior calculations were assumed to be random from day to day and uncorrelated with fuel moisture. Only weak autocorrelation of wind direction is suggested beyond 1 day [27]. Given the lack of spatial detail in wind flow over complex terrain (e.g., [14]), the additional effort required for obtaining and representing temporal wind dependencies was deferred for future consideration. Here, wind variability was characterized via the joint probability distribution of historical wind speed and direction as recorded by Remote Automated Weather Stations located near the fire for afternoon hours on days within the date range of the simulation (Fig. 1c). Daily values for wind speed and direction were sampled from this distribution for association with the fuel moisture values indicated by the ERC time series. This approach assumes that wind probabilities are constant throughout the simulation period (e.g., a few weeks) and not subject to low-frequency (i.e., seasonal) shifts.

A forecast period is the final element of the weather input stream. For use on actual wildland fires, weather forecasts for 1 to 7 days are continuously updated at specific weather stations from the National Digital Forecast Database (NDFD, http://www.nws.noaa.gov/ndfd/). The NDFD forecast is inserted into the weather data stream

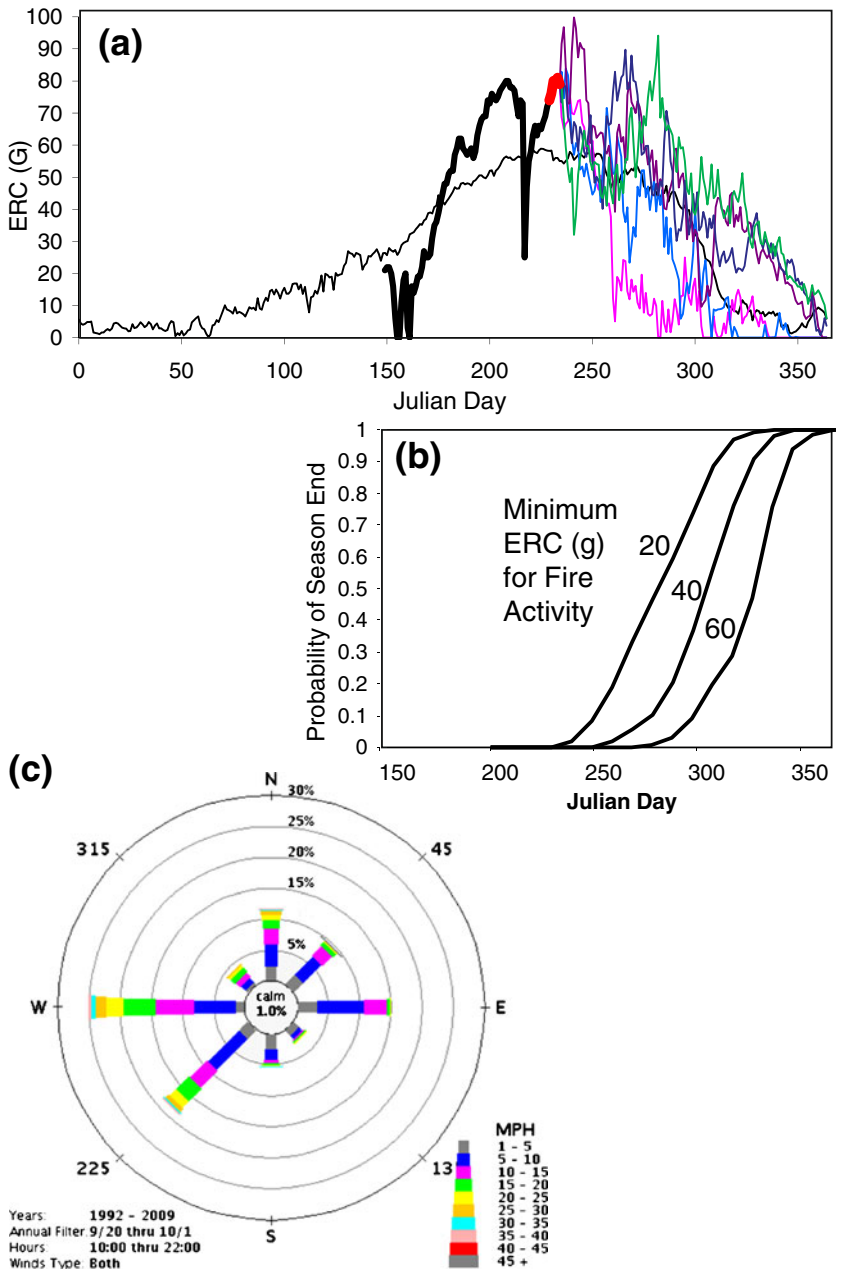


**Fig. 1** Illustrations of weather input for the ensemble simulation from the Uhl Hot Springs weather station in southern California. **a** The average seasonal trend (*thin black line*) and observations of the current year up to the simulation date (*bold black line*) and weather forecast (*bold red segment*) are used to generate synthetic sequences into the future (*colored lines*). **b** The probability of a season ending event is determined from 10,000 simulation years based on the specified lower ERC limit for fire spread. **c** Joint probability of wind speed and direction (shown here in the form of a "wind rose") is used to stochastically assign winds to each day in the simulation period

**Table 1** Example input table for ensemble fire simulations showing categories of fuel moisture content (MC) by ERC(G) percentile and related information used for fire behavior calculations

| ERC %tile | Min ERC(G) | Max ERC(G) | 1 h MC% | 10 h MC% | 100hMC% | Live herbaceous MC% | Live woody MC% | Burn period (min) | Spot prob. |
|---|---|---|---|---|---|---|---|---|---|
| 97–100 | 78 | 92 | 3.2 | 3.6 | 5.2 | 50 | 70 | 360 | 0.15 |
| 90–96 | 69 | 78 | 3.6 | 4.3 | 6.5 | 65 | 80 | 300 | 0.10 |
| 80–89 | 62 | 69 | 4.6 | 5.3 | 7.8 | 75 | 90 | 240 | 0.05 |
| 70–79 | 55 | 62 | 5.0 | 5.8 | 8.7 | 85 | 110 | 180 | 0.01 |
| 60–69 | 49 | 55 | 6.0 | 6.9 | 10.0 | 100 | 120 | 120 | 0.00 |

ERC(G) is the energy release component of the US National Fire Danger Rating System for fuel model "G"

after the last day of observed weather (i.e., when fire growth simulation begins). The simulated weather is generated to cover the period beyond the NDFD forecast. In other words, forecast ERC information is appended to the antecedent observations and used in the subsequent time series generations beyond the forecast. The wind speed and direction forecast are substituted for the random selections from the wind table for the forecast period.

## 4 Fire Simulation

Fire simulations were performed using a minimum travel time algorithm [21]. The algorithm simulates fire growth by calculating the time required for fire to travel from the ignition source(s) to nodes or points on a regular lattice covering the landscape. The travel time technique seeks the shortest-in-time straight-line travel paths among nodes of the lattice (Fermat's principle). The algorithm implemented by Finney [21] calculates travel times to nodes at any distance until a threshold condition is reached and "discourages" the algorithm from continuing. This discouragement threshold is defined by a number of sequential failures of the algorithm to find shortest-time paths. By limiting the shortest-path search in this way, distortions to fire shapes are minimized compared to results from algorithms that limit calculations among a fixed set of adjacent nodes [33, 35]. Thus, this algorithm produces the same fire shapes as wave-front expansion using Huygens' principle [5, 21]. The original algorithm [21] was modified to allow time-varying weather conditions (Fig. 2) and spotting from torching trees [2] and, thus, forces the spread rate along the straight-line paths to change with environmental conditions and spatial variables (i.e., cell boundaries). Fire spread rate and intensity are recorded at each node to allow analysis of fire behavior patterns within the burned area (Fig. 2b). Fire suppression actions are not considered by the simulation.

For computational efficiency, fire growth simulation required pre-calculation of fire behavior for the entire landscape under all combinations of moisture and wind speed and direction described above. These fire behavior calculations [20, 24] yield the spread and intensity of surface fire [38], crown fire [40, 47], and spotting distances from torching trees [2] provided the fuels, topography, and weather parameters. Spatial information on fuels and topography for all fires was obtained at 30-m resolution from the LANDFIRE project (http://www.landfire.gov). Data layers include descriptions of surface fuels [44] and canopy fuels in formats required by fire growth simulation software [20, 24]. Pre-processing of fire behavior improved the efficiency of this simulation system because the calculations could be parallelized and the results stored for repeated

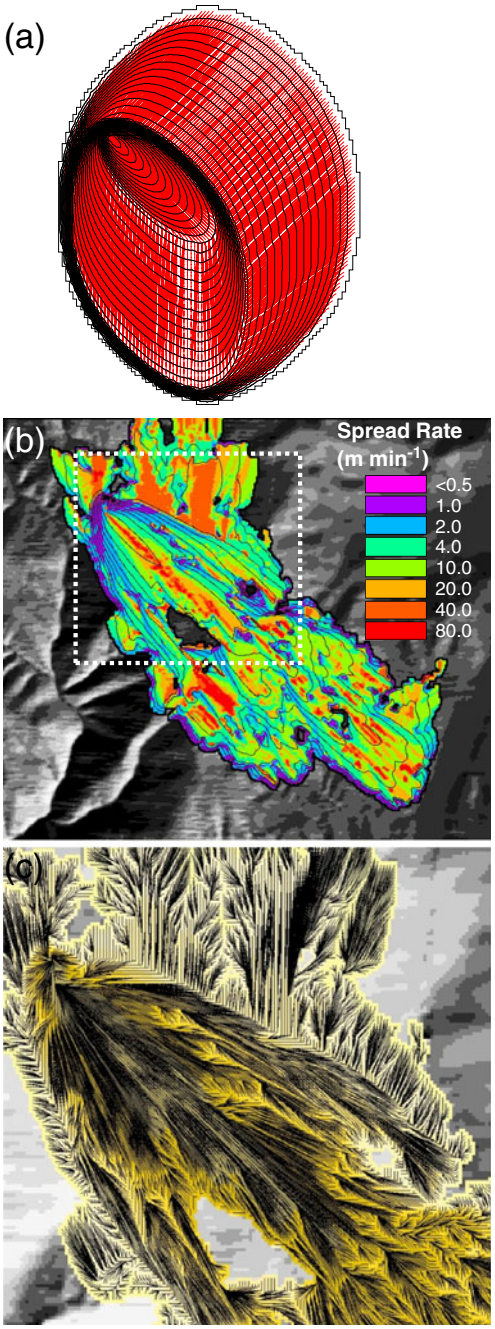


**Fig. 2** Demonstrations of the minimum travel time fire growth simulation. **a** Fire progression (*black time contours*) and travel paths (*red lines*) on flat terrain with constant fuels but varying wind directions (NW, N, and SW) result in minimal distortion of elliptical fire shape. **b** Complex terrain with temporally varying weather conditions showing fire spread rate within the fire perimeter. **c** Close-up of fire travel pathways from *inset* in **b** showing varying path lengths and directions

access by the fire growth algorithm for all of the many fires simulated in the ensemble. Only the data essential for fire growth and intensity were stored for each condition. These include the elliptical fire dimensions [21], direction of

maximum spread, maximum fire line intensity [15], and maximum spotting distance and direction. The index to the data stored for each of these fire behavior conditions was then referenced by the sequence of daily conditions produced for each of the artificial weather time series.

The ensemble simulation system was developed for shared-memory computers and parallelized with multi-threading among the independent Monte Carlo scenarios. Computers used for the simulations contained 16 or 32 processors with 32 to 64 GB of shared memory. Computing times were dependent on the number of simulations, the resolution of the spatial data, and the sizes of the fires, but most simulations were capable of achieving run times of no more than about 6 h.

## 5 Methods for Evaluating Model Performance

The ensemble fire simulation, called Fire Spread Probability (FSPro), was implemented in the Wildland Fire Decision Support System (WFDSS, http://wfdss.usgs.gov). WFDSS is a fire management system administered by the US Forest Service and Department of Interior and allows users to perform fire behavior calculations and document decisions in fighting or managing wildland fires. Ensemble results were obtained from WFDSS for purposes of evaluating FSPro performance. The results represent model performance under operational conditions on active fires. Sources of variability in the operational simulations originate from various sources. These include the choices made by different fire analysts who performed the simulations, such as the selected weather station, length of the time period, number of ensemble members, length of forecast period included, and any editing of the LANDFIRE fuel data based on input from local experts. Most fires are influenced to some degree by suppression actions that cannot be known with spatial or temporal specificity (e.g., line construction and burnout operations) or in terms of consequences to fire movement. The data set included 37 fires from 2007, 25 fires from 2008, and 29 fires from 2009 (Appendix 1) and only fires that remained active through the simulation period (e.g., a 14-day simulation must have active fire remaining on the 14th day and not successfully suppressed or declared contained prior to that). To warrant the attention of analysts, these fires were also among the largest and had the most potential for impacting valuable assets. It was recognized that selecting only these fires could bias the sample used for comparison by eliminating all fires that were smaller and extinguished earlier (i.e., naturally). However, without data on suppression actions, it was thought a lesser source of bias to exclude fires that may have been extinguished before the end of the specified simulation period.

We evaluated the accuracy of the ensemble simulations in two ways. First, for non-spatial evaluation, the observed size of each fire was plotted against the mean size of the ensemble members. Second, the ensemble probability field was evaluated by tabulating the frequency of intersections between observed fire perimeters and ensemble probability values. This second metric assumed that predictive agreement would be indicated if fires burn to a particular probability region in proportion to the predicted probability. For example, 10% of the fires should just reach the 0.10 ensemble probability contour, and 60% should just reach the 0.60 probability contour. To obtain the data for this comparison, for each fire, we overlaid the final fire perimeter polygon on the simulated burn probability grid and obtained the burn probabilities associated with each vertex of the polygon. The perimeter vertices are then sorted by the predicted ensemble burn probabilities to obtain percentile numbers of vertices (representing percentages of the fire perimeter). With data from all fires, we used the 100th percentile to make an extreme-case comparison (the minimum value of the ensemble probability that was intersected by the observed final perimeter). In other words, 100% of the perimeter vertices on a given fire had ensemble probabilities greater than this or equal to this value. The frequency of these intersections were then tallied within ensemble probability deciles and plotted relative to the ensemble probability. Second, we applied the same procedure to the 90th percentile perimeter vertex probability. This represents the frequency of fires each with 90% of their perimeter vertices equal to or greater than a particular ensemble probability.

The effect of simulation number on the precision of the ensemble calculations was explored by replicating the ensemble calculations with 256, 1,024, and 4,096 members. With six replicates for each ensemble number, the coefficient of variation (CV) was calculated for each pixel in the probability field using the observed counts (numbers of times the fire in the member simulation arrived at each cell). The CV was then plotted for each pixel by the average burn probability of the six simulations.

Comparisons of burn probability produced by 1D fire spread calculations with 2D fire growth calculations were made using an artificial test suite with a uniform landscape (constant fuels and flat terrain) and weather variability controlled by the number of wind directions. The weather scenarios consisted of random selections of wind speed and direction for each of two periods for each fire in the ensemble. Four wind speeds were available for all simulations (5, 10, 15, and 20 mph), but ensembles of 2,048 members were produced by varying the available wind directions. Tests included eight directions (0°, 45°, 90°, 135°, 180°, 225°, 270°, 315° azimuth), four directions (45°, 90°, 225°, 270°), and two directions (45°, 225°). The

2D probability fields from each of these ensembles were sampled along transects oriented along their major and minor axes and compared with results of 1D harmonic mean fire spread calculations [26, 30] in these same directions.

## 6 Results

Time series modeling was capable of generating a large number of realistic weather scenarios needed for the ensemble fire simulations and capturing the main influences of antecedent and future weather trends. A large ensemble sample size was required because fire growth is sensitive to the order of weather events, and there were large numbers of weather permutations within the typical time frame of 1 to 2 weeks. A typical set of weather conditions includes five fuel moisture categories (Table 1) and 49 wind combinations (direction by speed, including the singular category of calm), for a total of 245 possible daily weather conditions. By extension, a 7-day simulation is subject to $245^7$ possible sequences. The time series approach also incorporated the important long- and short-term trends in fuel moistures from the current year into the weather scenarios generated. In other words, the fire simulations are dependent on the antecedent trends in ERC (fuel moistures) prior to the day of the simulation, meaning the ensembles are sensitive to annual variation in fire season. Synthetic ERC time series show wide variation in daily values as well as annual trends (Fig. 1a). Annual variation produces probability distributions for the season ending date (Fig. 1b) based on the requisite minimum ERC identified for fire spread [28]. The wind variability represented by the joint probability distribution for wind speed and direction strongly influences the direction and magnitude of fire behavior and fire growth (Fig. 1c).

Variability of the ensemble fire growth simulations produced by the synthetic fire weather scenarios can be expressed in several ways, including a probability field of fire impact for the specified time period (Fig. 3a). Probability was estimated simply as the fraction of the total simulations where fire arrives at a particular cell. The fire size distribution summarizes the variability in total burned area during the simulation and is typically right-skewed (Fig. 3b). Each cell within the burn probability field has a probability distribution of arrival day, displayed as the conditional probability of the fire arriving on each day (Fig. 3c–e). The conditional probability of flame length (Fig. 3f–h) is but one demonstration of the variability in fire behavior that can occur as a result of (1) different burning conditions (fuel moisture, wind speed, and wind direction) as the fire encounters a particular cell, as well as (2) the trajectory of fire travel as it impacts a particular cell (producing heading, flanking, or backing spread into each). The individual "fire footprint" (grid data for each event, containing fire behavior values) can also be stored; but in this example, such would require considerable memory or disk space and subsequent effort to properly archive 2,016 separate gridded data sets from the ensemble members.

The number of simulations used for the ensemble affects the repeatability of the results. For the probability output field, the CV plotted on semi-log axes across the range of mean burn probabilities shows an S-shaped trend (Fig. 4a). The CV is relatively low within cells near the fire-start location, which have high burn probabilities (approximately >0.90), increases and generally plateaus for mid-range probabilities (~0.1 to ~0.9), and then increases rapidly for the lowest burn probability tails (approximately <0.1). The increase in simulation number from 256 to 4,096 decreased the CV across the entire range of average burn probability and enhanced estimates of lower probabilities as emphasized by log–log transformation (Fig. 4b).

The use of 2D fire simulations was found to provide substantial improvement in estimates of burn probability by comparison to 1D calculation. Even under the spatially homogenous conditions of these comparisons (i.e., constant fuel, flat terrain), travel along a 1D transect underestimated the probability of fire reaching a particular distance away from the ignition source (Fig. 5). The contrast between 1D and 2D was greatest with omni-directional wind variation (Fig. 5a). The greater variety of fire travel routes reduced 1D probability equally in every direction. As wind direction was increasingly restricted, the contrast between 1D and 2D calculations heightened along the major axis of spread direction (the "a" direction in Fig. 5b, c). Ultimately, the 1D and 2D spread probabilities converged along the major axis when wind variability was confined to only two directions (180° oscillations). Along the minor axis of spread, however, probabilities from 1D were always lower than 2D calculations (direction "b" in Fig. 5b, c).

Ensemble results for wildland fires from 2007, 2008, and 2009 were compared with observed fire growth between the start and end date of the simulation (Fig. 6). Such comparisons cannot individually indicate the accuracy of the probabilistic predictions, but collectively reveal strong correlations with both predicted sizes and modeled probabilities (Fig. 7). Mean sizes of simulated fires tended to be greater than those observed (Fig. 7a). With all vertices considered (i.e., 100th percentile), the ensemble simulation tended to underestimate burn probability (Fig. 7b). Agreement was better using the 90th percentile vertex probability (Fig. 7b), indicating a strong influence from small portions of observed fire perimeters. Such influence is evident in Fig. 6a–c, which show cases in which narrow segments of the final fire perimeter extend, finger-like, well into areas of low burn probability from the ensemble simulations.

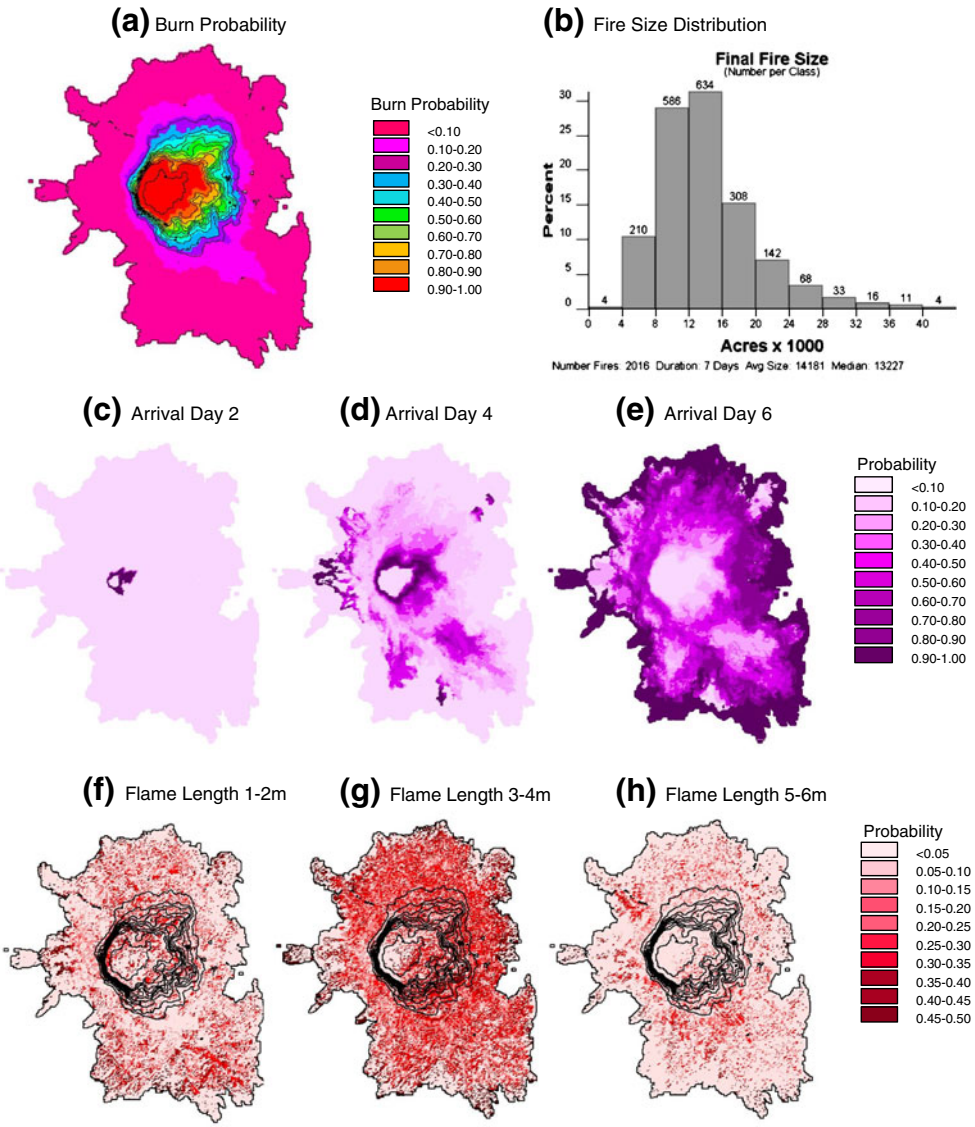


**Fig. 3** Example results of FSPro ensemble simulations. **a** Ensemble burn probabilities are depicted for the specified time period (shown here 7 days). **b** The fire size distribution from the ensemble members is typically right skewed. Also produced are probabilities of fire arrival for each day in the simulation period, for example: **c** day 2, **d** day 4, and **e** day 6. The variability in fire behavior can be depicted as the probability of flame length of **f** 1–2 m, **g** 3–4 m, and **h** 5 to 6 m

## 7 Discussion

The FSPro simulation process produced ensemble estimates of 2D fire growth that showed substantial agreement with observed fire perimeters from 91 fires. Validation of ensembles is complicated by the inability to make direct observation of probabilities, relying on frequencies of observations instead. Trends among these frequencies implied that the ensemble average fire size was larger than the observed final fire size (Fig. 7a), and the simulated fires reached less in maximum extent than the observed fires (Fig. 7b). Fire size trends might be explained by the extinguishment of portions of the fire perimeter that are not modeled. These can occur naturally but primarily because of suppression actions mostly in backing (rear) or flanking (lateral) directions. In these cases, only part of the fire edge produces increases in burned area, thus, leading to over-prediction of total burned area. With right-skewed distributions of fire sizes (Fig. 3b), the use of the ensemble mean is, however, a somewhat arbitrary reference for comparison with final perimeters (could use median or mode) and is an indication of consistency more than accuracy. Overprediction of burned area may also be a result of greatly simplified wind conditions used in simulations as Anderson et al. [4] reported. If so, then improvements may be found in more sophisticated modeling of wind changes (e.g., [32]) or in use of gridded wind fields (e.g., [14]).

Maximum fire extent occurs in the spread direction with the greatest fire growth and, presumably, has the most resistance to fire suppression efforts. Thus, the apparent underprediction of fire extent may be related to different factors, such as the exclusive use of fires considered active

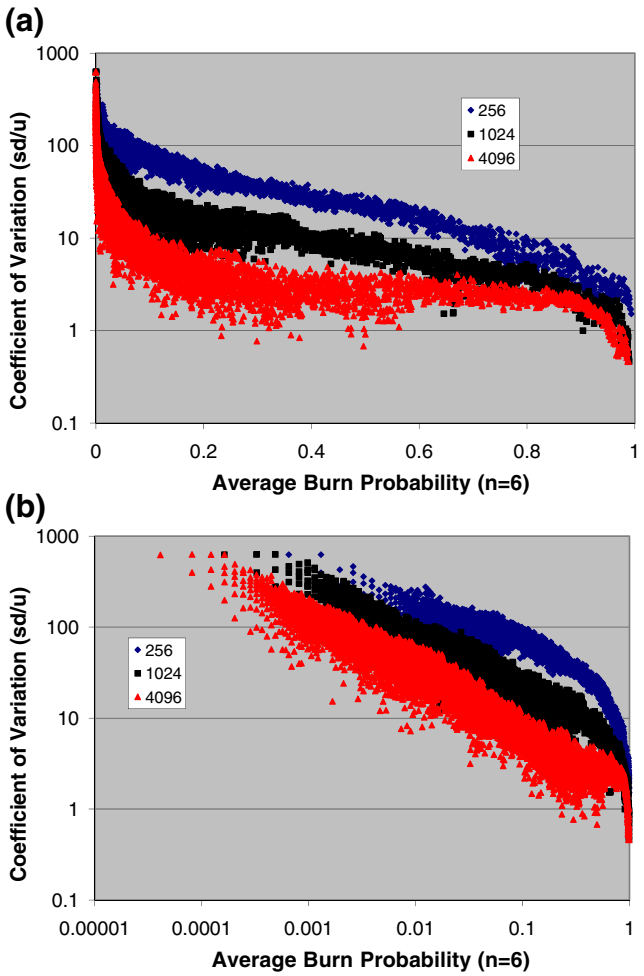


**Fig. 4** Effects of the number of ensemble fire simulation members on the CV. Six replications of a 7-day simulation were made for each ensemble sample number (256, 1,024, and 4,096), and the CV was determined from counts of fire occurrence in each cell. On semi-log axes (**a**), the CV is seen to rise from the lowest values near burn probability of 1.0 and plateau or rise gently over the mid-range of the burn probabilities (0.1–0.9) before increasing dramatically because of the low sample sizes associated with the low burn probabilities. On log–log axes (**b**), the CV trends for the lowest burn probabilities clearly reveal the effect of sample sizes on the lower range of estimated burn probabilities and the improvement in repeatability for these low probabilities from increased ensemble numbers

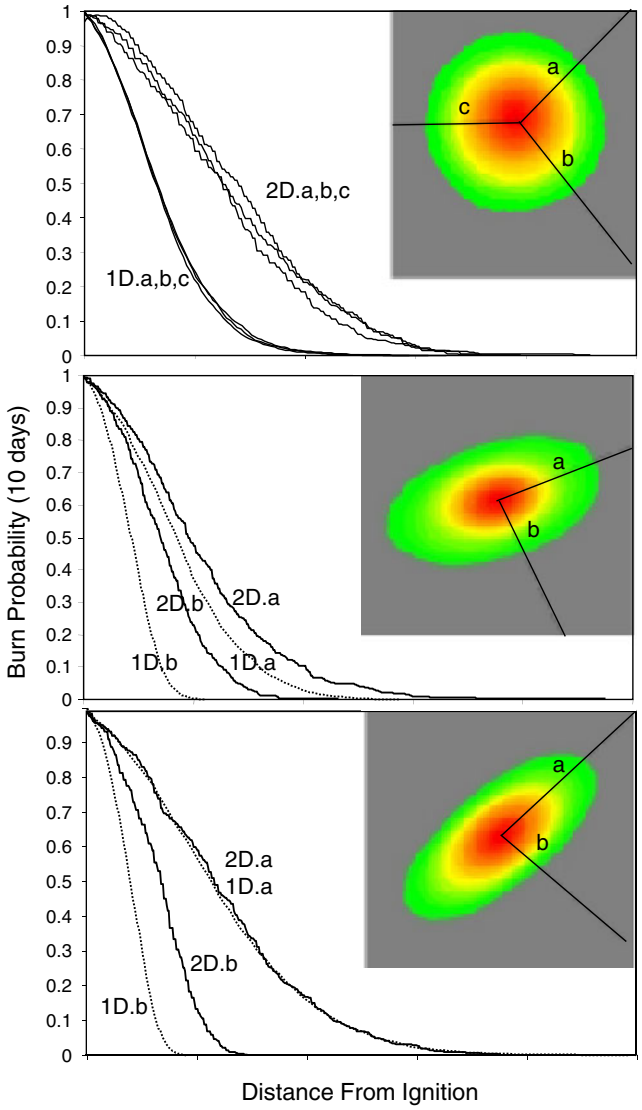


**Fig. 5** Illustration of burn probability from two-dimensional (*2D*) fire growth calculations and one-dimensional (*1D*) fire spread calculations where spread directions vary. Landscape is uniform, and ignition is from single point source. **a** Allowing wind directions to vary randomly from eight directions produces a circular burn probability field which always indicates greater probabilities at a particular distance than calculations made by 1D methods. **b** Restricting the simulations to four wind directions (45, 90, 225, and 270) limits the spread variability and brings the 1D and 2D estimates closer, particularly along the major axis of spread. **c** With only two directions of spread (45, 225), the 1D and 2D probabilities are the same along the major axis but remain very different along the minor axis

for the full simulation period and the use of burnout operations as part of suppression actions. Suppression activities on larger fires often remove fuels ahead of fires by igniting from an established fireline. This tends to advance the fire edge more rapidly than would occur naturally. However, the difference between the 100th percentile (minimum probability) and the 90th percentile results (Fig. 7b) may reflect the influence of localized fire activity along a few segments of the active fire perimeter (Fig. 6) which extend to predicted probability zones more frequently than predicted. Numerous explanations might be proposed that relate to fine-scale variability in fire environment (small valleys, local wind currents, or fuel patches) not resolved by the simulation, possibly by localized suppression action or because the ensemble sample size of weather inputs (Appendix 1) are insufficient to capture rare

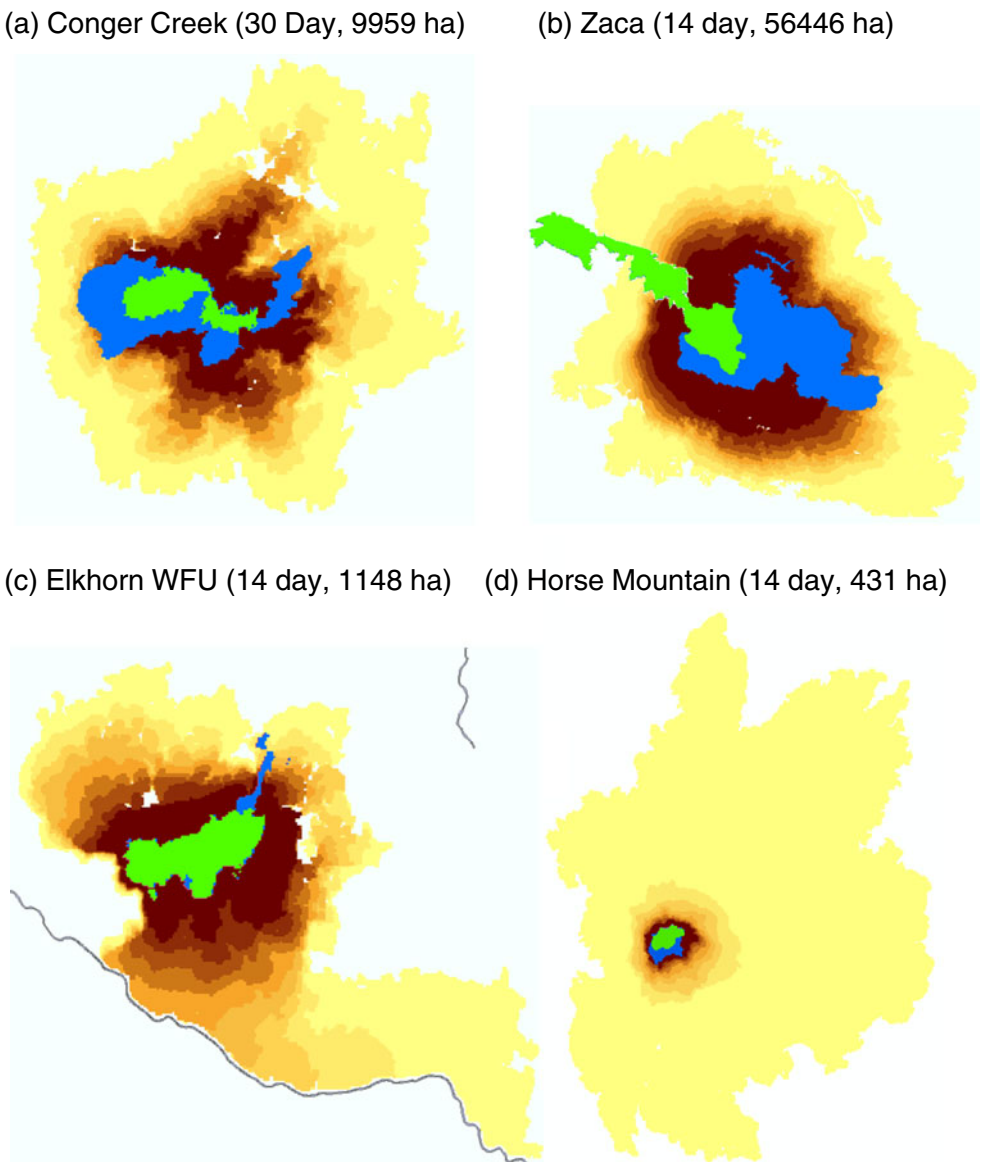


**Fig. 6** Examples of observed fire perimeters overlaid on ensemble probability fields simulated by FSPro. The observed fire area at the beginning and end of the simulation is indicated by *green* and *blue shading*, respectively. **a** through **c** show examples of fires that spread mainly in narrow "fingers" rather than along broad fronts

wind events experienced by the fire. The uncertainty and variation caused by fine-scale weather and fuels on fire behavior could possibly be captured for the FSPro simulation using methods similar to those described by Boychuk et al. [10]. However, validation of fire simulation in general is made difficult by the multiple sources of error that are confounded with the error of the model itself. These include the accuracy of spatial fuels information, bias in weather station locations compared to where the fire is burning, and mapping of fire perimeter locations. Other errors in an operational system involve the user or analyst who runs the models and whose judgment is required to make model settings (e.g., choice of weather station, use of weather forecasts, and adjustments to fuel maps).

The ensemble burn probability fields (Fig. 3a) have specific interpretations that can be counterintuitive:

- The fields portray the independent burn probability of each geographic location in the simulation domain (i.e., probability is estimated by tallying fire overlap for each cell in the landscape independently). The burn probabilities are useful for estimating fire impact on independent values (e.g., homes) in a risk assessment framework.
- The probability field implies no time frame for burning other than the specified limit of the simulation period

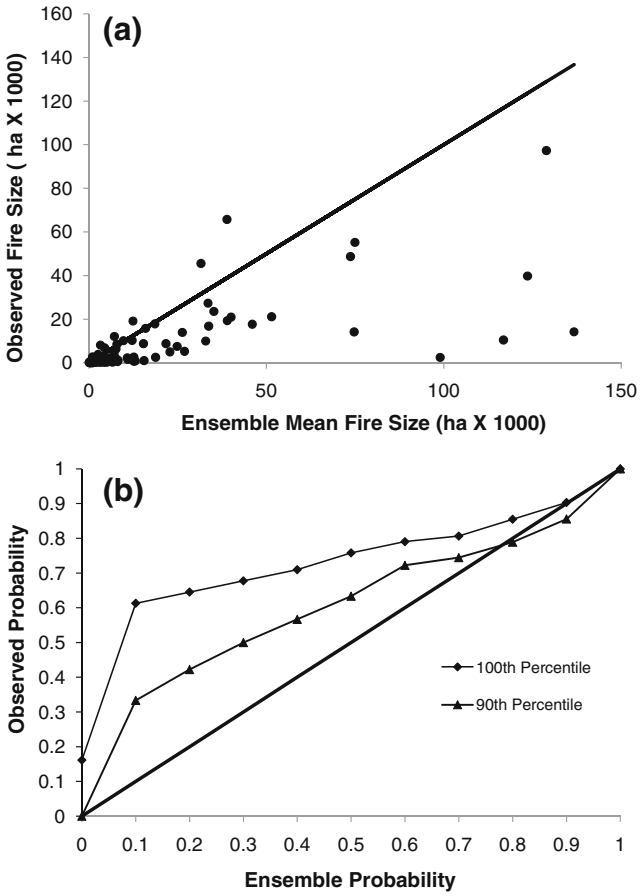


**Fig. 7** Comparisons of 91 wildland fires were made against ensemble simulation results in terms of **a** the mean size of observed and simulated fires and **b** the probability of observed and simulated maximum fire extent. Observed fire sizes (area) tended to be consistently smaller than the average simulated fire size (**a**), but the maximum fire extent occurred at higher probabilities (frequencies) than predicted (**b**)

(between the start and end dates). Variability in arrival day for each geographic location can also be obtained from the simulation (Fig. 3c–e).

- Probability contours indicate nothing about the fire routes of travel or direction to any location. Fire growth across the landscape is different among ensemble members and produces a mix of heading, flanking, and backing spread as well as spotting from the main fire front which produces fire behavior variation (Fig. 3f–h).
- Nothing about the expected shape or the size of a single fire can be interpreted from the burn probability field because the fire growth simulation members have different shapes and sizes. For example, an 80% probability contour indicates only that there is an 80% chance of the fire reaching any point on that contour. The shape or skew of the probability field, however, does reveal the influence of predominant wind directions.
- Incorrect interpretations with regard to the 80% probability contour, for example, include:
  - 80% of the fire will be inside the area delineated by the contour
  - The area within the contour has at least an 80% chance of burning
  - The fire has an 80% chance of having a size equal to the area within the contour

Greater ensemble sample sizes reduced variability of the estimated burn probabilities and would presumably lead to more reliable estimates of expected impacts for quantitative risk assessment, especially in the mid-range of burn probabilities (0.1–0.9, Fig. 4a). The CV remained relatively stable over this mid-range with the largest ensemble sample of 4,096 members but indicated (by the sloping trend) that rare weather events were poorly captured by lower ensemble numbers of 1,024 and 256. The rapid rise in CV below a burn probability of about 0.1 (Fig. 4a) suggests that rare weather events or sequences have strong effects on the estimated probabilities and that large sample sizes would be required to achieve repeatable estimates of these low probabilities. This analysis could not determine an optimum or recommended sample size but does indicate a need for many thousands of ensemble members to produce repeatable quantitative estimates. Smaller sample numbers may be acceptable if the simulation is intended for qualitative demonstration of uncertainty or if the probability threshold for fire impact is relatively high (e.g., above 0.5). If high confidence is required for estimating very low probabilities (e.g., less than 0.01), then sample sizes would have to be considerably larger than tested here (Fig. 4b). Very high sample numbers would be more likely to contain the rarest combinations of weather conditions and thus be useful for depicting a wider range of potential fire impacts that, although unlikely, could have major consequences.

The use of 2D simulation for the heterogeneous fire environment provided a substantial improvement over strict 1D calculations (Fig. 5) by virtue of accounting for the predominance of indirect spread paths across the landscape under variable conditions (in either time or space). The assumption in strict 1D spread calculations is that the shortest-time path between two points is a straight line, when, under heterogeneous conditions, the fastest route clearly involves multiple segments that arrive sooner by an indirect path. The demonstration in Fig. 5 for time-varying factors shows that the 1D and 2D calculations are the same along the major axis (heading-backing direction) only if the spread can alternate just between 180° options.

Fire spread for 1D and 2D spread in flanking directions was never identical. This contrast between 1D and 2D for time-varying conditions is consistent with the effects of spatial variability on fire spread rates [22]. Fire spread through two-dimensional, spatially random fuel mixtures was underestimated by 1D harmonic averages of the component spread rates [16, 26] compared to 2D simulation. The downside to 2D calculation, however, is increasing intensiveness of computing and associated processing time.

The time series analysis was a valuable method for accounting for critical weather trends and variables affecting fire behavior beyond the time frames of weather forecasts. The simulation and the time series technique is sensitive to variation in weather trends specific to certain climate regions such as the bimodal fire season common to the Southwest [42]. The time series analysis also preserves the uniqueness of the current year's observations, meaning that ensemble probabilities would be different from year-to-year for the same fire location and date. Time series modeling also provided a method of determining the distribution of season-ending events [28], which curtail fire growth (i.e., due to frequent precipitation, Fig. 1b). Wind probabilities that could vary seasonally were modeled separately from the fuel moisture trends and captured by restricting the time range filter to dates overlapping with the simulation period.

## 8 Conclusions

The techniques described here offer the initial capability to perform risk assessments for individual wildland fires. Time series analysis was appropriate for assessment of trends in fuel moisture and the associated fire danger rating index (ERC) because of the long time lags associated with the component fuel size classes. By way of this analysis, we were able to assess and account for trends in moisture content in the current year, simulate the large numbers of potential sequences needed for generating fire probabilities, and generate a probability distribution of season-ending dates. Potential improvements to the predictions from adding ensemble forecasts for the days preceding the time series will be evaluated in the future. We found that the computing requirements for the two-dimensional calculation were reasonable, involving the use of relatively inexpensive multi-core and multi-processor computers. Compared to one-dimensional calculations, 2D modeling improves both the display and accuracy of fire simulations in heterogeneous spatial environments. Evaluated against data from 91 fires, the ensemble burn probabilities showed consistent agreement with the fire size observations.

**Acknowledgements** The authors gratefully acknowledge the financial support facilitated by John Syzmoniak of the US Forest Service Washington Office division of Fire and Aviation Management. Larry Bradshaw provided advice and technical assistance with weather data and analysis. Karen Short offered many helpful comments.

## 1. Appendix

**Table 2** Data on wildland fire incidents in 2007, 2008, and 2009 and FSPro ensemble simulation settings used for comparisons of model performance

| Incident name | State | Date | Spatial resol. (m) | Number of ensemble members | Duration (days) | Mean FSPro size (ha) | Final size (ha) |
|---|---|---|---|---|---|---|---|
| Ahorn | MT | August 10, 2007 | 200 | 600 | 30 | 51,477 | 21,082 |
| ANF Station | CA | August, 29, 2009 | 120 | 3,008 | 7 | 74,959 | 55,189 |
| Battle | ID | August, 10, 2007 | 120 | 1,008 | 17 | 10,949 | 1,544 |
| Beaverdam | WY | August 1, 2007 | 60 | 3,000 | 30 | | 5,109 |
| Bering Creek 2 (395) | AK | July 7, 2009 | 90 | 2,016 | 12 | 18,584 | 17,849 |
| Bitteroot WFU | ID | March 11, 2007 | 90 | 1,008 | 14 | 24,845 | 7,490 |
| Boze_9237 | OR | September 13, 2009 | 30 | 5,024 | 6 | 430 | 647 |
| Bridge | ID | August 10, 2007 | 200 | 600 | 30 | 46,014 | 17,684 |
| Brush Creek | WA | August 2, 2009 | 30 | 5,024 | 6 | 210 | 158 |
| Brushcreek | MT | August 8, 2007 | 120 | 2,000 | 14 | | 12,081 |
| Cabin Creek | ID | August 4, 2008 | 60 | 3,008 | 14 | 7,646 | 1,820 |
| Calbick | MT | August 18, 2007 | 90 | 1,000 | 14 | 5,089 | 308 |
| Chain | ID | August 10, 2007 | 120 | 1,008 | 14 | 8,045 | 540 |
| Chippy | MT | August 7, 2007 | 200 | 600 | 14 | | 39,201 |
| Conger Creek | MT | August 10, 2007 | 180 | 600 | 30 | 32,888 | 9,959 |

**Table 2** (continued)

| Incident name | State | Date | Spatial resol. (m) | Number of ensemble members | Duration (days) | Mean FSPro size (ha) | Final size (ha) |
|---|---|---|---|---|---|---|---|
| Corporal | MT | August 19, 2007 | 90 | 1,000 | 30 | 7,600 | 6,297 |
| Cougar | NM | July 27, 2009 | 60 | 5,008 | 11 | 187 | 126 |
| Devil WFU | CA | November 5, 2007 | 45 | 4,000 | 25 | 60 | 85 |
| Diamond | NM | May 28, 2009 | 90 | 2,016 | 16 | 22,814 | 4,987 |
| Ditch Creek | WY | August 29, 2009 | 30 | 5,024 | 7 | 320 | 9 |
| Dog | ID | August 10, 2007 | 120 | 1,008 | 17 | 26,932 | 5,255 |
| Domke Lake | WA | August 5, 2007 | 30 | 1,008 | 25 | 2,585 | 3,817 |
| Drake | ID | August 10, 2007 | 120 | 1,008 | 17 | 12,638 | 2,613 |
| El Cap | ID | August 12, 2007 | 90 | 1,008 | 14 |  | 1,871 |
| Elkhorn | ID | August 12, 2007 | 90 | 1,008 | 14 | 8,198 | 1,148 |
| Fish WFU | UT | August 9, 2008 | 60 | 3,008 | 21 | 351 | 74 |
| Fool Creek | MT | August 9, 2007 | 60 | 1,000 | 14 | 35,206 | 23,536 |
| Grants–Babcock | CA | July 20, 2007 | 60 | 2,000 | 14 | 272 | 72 |
| Grants–Babcock | CA | July 20, 2007 | 60 | 3,008 | 30 | 611 | 41 |
| Grizzly | ID | August 10, 2007 | 120 | 1,008 | 17 | 15,515 | 973 |
| Gunbarrel | WY | August 3, 2008 | 60 | 2,016 | 14 | 33,725 | 16,764 |
| Gunsight | WY | September 27, 2009 | 30 | 4,000 | 6 | 2,211 | 1,326 |
| Harrington | ID | August 12, 2007 | 90 | 1,008 | 14 | 98,966 | 2,458 |
| Hell's Half Saddle | MT | August 7, 2008 | 60 | 3,008 | 30 | 6,620 | 255 |
| Horse Mountain | OR | August 22, 2008 | 90 | 2,016 | 10 | 2,632 | 431 |
| Hot Air | AZ | June 24, 2008 | 120 | 3,008 | 7 | 7,051 | 3,931 |
| Jack WFU | CA | October 29, 2007 | 45 | 4,000 | 20 | 104 | 227 |
| Jagged Ridge (497) | AK | July 26, 2009 | 90 | 4,000 | 7 | 40,053 | 20,931 |
| Jocko Lakes | MT | August 7, 2007 | 200 | 600 | 14 | 74,733 | 14,143 |
| KNF Bear Wallow Complex: Milne | CA | July 10, 2008 | 90 | 2,016 | 30 | 12,616 | 689 |
| KNF Panther | CA | July 25, 2008 | 90 | 3,008 | 21 | 15,345 | 8,748 |
| KNF Siskiyou Complex | CA | July 1, 2008 | 90 | 3,008 | 14 | 15,954 | 15,767 |
| Kootenai | MT | July 12, 2009 | 30 | 3,008 | 14 | 3,442 | 823 |
| Lake Fork | UT | July 2, 2009 | 60 | 4,000 | 14 | 3,245 | 208 |
| Lemah | WA | July 25, 2009 | 60 | 2,016 | 35 | 2,097 | 209 |
| Little Black One (314) | AK | June 21, 2009 | 90 | 200 | 21 | 116,840 | 10,424 |
| Little Mud (417) | AK | July 10, 2009 | 90 | 3,008 | 16 | 12,395 | 19,134 |
| Lizard | ID | August 10, 2007 | 120 | 1,008 | 17 | 18,755 | 2,522 |
| Lonesome | OR | September 7, 2008 | 90 | 2,016 | 7 | 1,557 | 1,723 |
| Lonesome | OR | September 7, 2008 | 90 | 2,016 | 21 | 3,237 | 8,111 |
| LPF Basin Complex | CA | July 3, 2008 | 120 | 4,000 | 11 | 73,692 | 48,740 |
| Magruder | ID | August 12, 2007 | 90 | 1,008 | 14 |  | 1,655 |
| Main | NM | July 21, 2009 | 30 | 4,000 | 14 | 351 | 112 |
| Meason | NM | June 1, 2009 | 30 | 4,000 | 10 | 949 | 2,226 |
| Mill Flat | UT | July 25, 2009 | 60 | 5,024 | 24 | 1,032 | 49 |
| MNF Yolla Bolly Complex | CA | June 28, 2008 | 90 | 2,016 | 7 | 3,283 | 1,836 |
| Moore | NM | July 11, 2009 | 60 | 3,008 | 30 | 2,077 | 1,634 |
| North Fork Wilderness Complex | OR | August 1, 2009 | 60 | 4,000 | 21 | 13,022 | 826 |
| Nowitna | AK | June 16, 2009 | 90 | 3,008 | 20 | 38,979 | 19,296 |
| Panther Creek | WA | June 28, 2009 | 30 | 5,024 | 14 | 852 | 85 |
| Pattengail_2 | MT | July 28, 2007 | 120 | 4,000 | 30 |  | 4,926 |
| Piute | CA | July 2, 2009 | 90 | 2,016 | 10 | 136,706 | 14,199 |
| PNF Canyon Complex: Cold | CA | June 23, 2008 | 90 | 3,008 | 14 | 10,780 | 2,232 |
| Railley | MT | July 16, 2007 | 120 | 1,000 | 30 | 21,688 | 8,739 |

**Table 2** (continued)

| Incident name | State | Date | Spatial resol. (m) | Number of ensemble members | Duration (days) | Mean FSPro size (ha) | Final size (ha) |
|---|---|---|---|---|---|---|---|
| Rambo Mtn | MT | July 31, 2007 | 90 | 700 | 30 | 9,702 | 10,137 |
| Rat Creek | MT | August 10, 2007 | 90 | 1,000 | 14 | 7,883 | 8,489 |
| Rat creek | MT | August 10, 2007 | 90 | 120 | 30 | 12,158 | 10,286 |
| Rattle | OR | September 7, 2008 | 90 | 2,016 | 14 | 4,380 | 6,881 |
| Rattlesnake | ID | July 13, 2007 | 200 | 600 | 30 | 123,623 | 39,747 |
| Rush Creek | ID | July 18, 2008 | 60 | 4,000 | 14 | 1,309 | 573 |
| Sable | WA | July 30, 2009 | 60 | 4,000 | 30 | 4,347 | 206 |
| Sawmill Complex | MT | July 18, 2007 | 90 | 1,000 | 30 | 33,545 | 27,319 |
| SHF Alp Complex: Granite | CA | June 26, 2008 | 90 | 4,000 | 7 | 1,555 | 177 |
| SHF Alp Complex: Clem, Buckhorn | CA | June 26, 2008 | 90 | 3,008 | 7 | 2,377 | 1,170 |
| Skyland | MT | July 23, 2007 | 150 | 1,000 | 14 | | 18,306 |
| Solomon Basin | UT | July 30, 2009 | 30 | 4,000 | 14 | 972 | 95 |
| SQF_Clover | CA | May 31, 2008 | 30 | 3,008 | 14 | 1,557 | 598 |
| SRF Blue 2 | CA | June 26, 2008 | 90 | 3,008 | 14 | 5,745 | 938 |
| SRF Ukonom Complex | CA | July 5, 2008 | 120 | 2,016 | 21 | 26,317 | 13,926 |
| Stevens Creek #1 | AK | June 18, 2009 | 60 | 4,000 | 8 | 7,146 | 12,057 |
| STF Dome Rock | CA | October 2, 2008 | 60 | 3,008 | 13 | 1,142 | 133 |
| Tie Fork | UT | August 26, 2009 | 60 | 5,024 | 12 | 545 | 332 |
| Titna River | AK | July 11, 2009 | 90 | 3,008 | 25 | 38,892 | 65,722 |
| Twin Hollow | UT | August 25, 2009 | 60 | 4,000 | 7 | 209 | 108 |
| Westy | ID | August 20, 2008 | 60 | 3,008 | 21 | 4,495 | 1,749 |
| Williams Creek | OR | July 28, 2009 | 60 | 5,024 | 10 | 1,043 | 2,665 |
| Wood Hump | MT | August 14, 2008 | 60 | 4,000 | 30 | 5,655 | 2,150 |
| Wood Hump | MT | August 6, 2008 | 60 | 4,000 | 7 | 2,146 | 891 |
| Zaca | CA | July 29, 2007 | 90 | 2,000 | 14 | | 56,446 |
| Zaca | CA | July 29, 2007 | 120 | 1,000 | 14 | 128,923 | 97,287 |
| Zitziana | AK | June 17, 2009 | 60 | 2,016 | 20 | 31,568 | 45,560 |

## References


1. Ager, A. A., Finney, M. A., Kerns, B. K., & Maffei, H. (2007). Modeling wildfire risk to northern spotted owl (*Strix occidentalis caurina*) habitat in Central Oregon USA. *Forest Ecology and Management, 246*, 45–56.
2. Albini, F.A. (1979). Spot fire distance from burning trees—A predictive model. USDA For. Serv. Gen. Tech. Rep. INT-56.
3. Anderson K.R., Flannigan M.D., & Reuter G. (2005). Using ensemble techniques in fire-growth modelling. In: 6th Symp. on Fire and Forest Meteorology, vol. 2.4. Canmore, Alberta Amer Meteorol Soc, Boston, MA, pp 1–6, 24–27, Oct 2005
4. Anderson, K., Reuter, G., & Flannigan, M. D. (2007). Fire-growth modeling using meteorological data with random and systematic perturbations. *International Journal of Wildland Fire, 16*, 174–182.
5. Andre, J. C. S., Urban, J. M., & Viegas, D. X. (2006). Forest fire spread models: The local quasi-equilibrium approach. *Combustion Science Technology, 178*(10–12), 2115–2143.
6. Andrews, P.L. (1986). BEHAVE: Fire behavior prediction and fuel modeling system—BURN subsystem Part 1. USDA For. Serv. Gen Tech. Rep. INT-194.
7. Andrews, P. L., Loftsgaarden, D. O., & Bradshaw, L. S. (2003). Evaluation of fire danger rating indexes using logistic regression and percentile analysis. *International Journal of Wildland Fire, 12*, 213–226.
8. Barrows, J.S. (1951). Fire behavior in the northern Rocky Mountain forests. USDA Forest Service Station Paper Number 29, 103 pages.
9. Box, G., & Jenkins, G. (1976). *Time series analysis: Forecasting and control*. San Francisco: Holden Day.
10. Boychuk, D., Braun, W. J., Kulperger, R. J., Kroughly, Z. L., & Stanford, D. A. (2009). A stochastic fire growth model. *Environmental and Ecological Statistics, 16*, 133–151.
11. Bradshaw, L.S., Deeming, D.A. Burgan, R.E., & Cohen, J.D. (1983). The 1978 National Fire-Danger Rating System: Technical documentation. United States Department of Agriculture, Forest Service, General Technical Report INT-169. Intermountain Research Station, Ogden, Utah, 44 pages.
12. Braun, W.J., Jones, B.L., Lee, J.SW., Woodford, D.G., & Wotton, B.M. (2010). Forest fire risk assessment: An illustrative example from Ontario, Canada. Journal of Probability and Statistics 2010, 823018, 26 pages
13. Brown, A. A., & Davis, K. P. (1973). *Forest fire control and use* (McGraw Hill series in forest resources). New York: McGraw-Hill. 686 pages.
14. Butler, B. W., Forthofer, J. M., Stratton, R. D., Finney, M. A., & Bradshaw, L. S. (2005). Fire growth simulations of the Price Canyon, Thirtymile, and Storm King mountain fire using high

resolution wind simulation tools and FARSITE. Sixth Symposium on Fire and Forest Meteorology, Oct. 25–27, Canmore, AB, Canada
15. Byram, G. M. (1959). Combustion of forest fuels. In K. P. Davis (Ed.), *Forest fire: Control and use*. New York: McGraw-Hill.
16. Catchpole, E. A., Hatton, T. J., & Catchpole, W. R. (1989). Fire spread through nonhomogeneous fuel modeled as a Markov process. *Ecological Modelling, 48*, 101–112.
17. Calkin D.E., Ager, A.A., Gilbertson-Day, J., Scott, J.H., Finney, M.A., Schrader-Patton, C., Quigley, T.M., Strittholt, J.R., & Kaiden, J.D. (2010). Wildfire risk and hazard: Procedures for the first approximation. US Forest Service, Rocky Mountain Research Station RMRS-GTR-235.
18. Colemen, J. R., & Sullivan, A. L. (1996). A real-time computer application for the prediction of fire spread across the Australian landscape. *Simulation, 67*(4), 230–240.
19. Deeming, J.E., Burgan, R.E., & Cohen, J.D. (1977). The national fire-danger rating system—1978. USDA For. And Range Exp. Station, Gen. Tech. Rep. INT-39.
20. Finney M.A. (1998). FARSITE: Fire area simulator—Model development and evaluation. USDA For. Serv. Res. Pap. RMRS-RP-4
21. Finney, M. A. (2002). Fire growth using minimum travel time methods. *Canadian Journal of Forest Research, 32*(8), 1420–1424.
22. Finney, M. A. (2003). Calculation of fire spread rates across random landscapes. *International Journal of Wildland Fire, 12*, 167–174.
23. Finney, M. A. (2005). The challenge of quantitative risk analysis for wildland fire. *Forest Ecology and Management, 211*, 97–108.
24. Finney, M.A. (2006). An overview of FlamMap fire modeling capabilities. USDA For. Serv. Gen. Tech. Rep. RMRS-P-41, pp. 213–220.
25. Fosberg, M.A. & Deeming, J.E. (1971). Derivation of the 1- and 10-hour time lag fuel moisture calculations for fire danger rating. United States Department of Agriculture, Forest Service, Research Note RM-207. Rocky Mountain Forest Experimental Station, Fort Collins, Colorado, 8 pages.
26. Fujioka, F. M. (1985). Estimating wildland fire rate of spread in a spatially non-uniform environment. *Forest Science, 31*(3), 21–29.
27. Kalvova, J., & Sobisek, B. (1981). Periodicity in time series of wind direction data. *Studia Geophysica Et. Geodaetica, 25*, 275–283.
28. Latham, D.J. & Rothermel, R.C. (1993). Probability of fire-stopping precipitation events. USDA For. Serv. Research Note INT-510, 8 pp.
29. Martell, D. L. (1999). A Markov chain model of day to day changes in the Canadian forest fire weather index. *International Journal of Wildland Fire, 9*(4), 265–273.
30. Martin, R. E. (1988). Rate of spread calculation for two fuels. *Western Journal of Applied Forestry, 3*(2), 54–55.
31. Massada, A. B., Radeloff, V. C., Stewart, S. I., & Hawbaker, T. J. (2009). Wildfire risk in the wildland -urban interface: A simulation study in northwestern Wisconsin. *Forest Ecology and Management, 258*, 1990–1999.
32. Negra, N. B., Holmstrom, O., Bak-Jensen, B., & Sorensen, P. (2008). Model of a synthetic wind speed time series generator. *Wind Energy, 11*, 193–209.
33. O'Regan, W. G., Kourtz, P., & Nozaki, S. (1976). Bias in the contagion analog to fire spread. *Forest Science, 2*(1), 61–68.
34. Parisien, M.G., Kafka, V.G., Hirsch, K.G., Todd, J.B., Lavoie, S. G., & Maczek, P.D. (2005). Mapping wildfire susceptibility with the BURN-P3 simulation model. Inf. Rep. NOR-X-405 Canadian Forest Service Northern Forestry Centre, 36 pages.
35. Peterson, S.H., Morais, M.E., Carlson, J.M., Dennison, P.E., Roberts, D.A., Mortiz, M.A., & Weise, D.R. (2009). Using HFire for spatial modeling of fire in shrublands. USDA For. Serv. Pac. Southwest Research Station, PSW-RP-259, 44 pages
36. Richards, G. D. (1990). An elliptical growth model of forest fire fronts and its numerical solution. *International Journal for Numerical Methods Engineering, 30*, 1163–1179.
37. Richards, G. D. (1999). The mathematical modelling and computer simulation of wildland fire perimeter growth over a 3-dimensional surface. *International Journal of Wildland Fire, 9*(3), 213–221.
38. Rothermel, R.C. (1972). A mathematical model for predicting fire spread in wildland fuels. USDA For. Serv. Res. Pap. INT-115.
39. Rothermel, R.C. (1983). How to predict the spread and intensity of forest and range fires. USDA For. Serv. Gen. Tech. Rep. INT-143
40. Rothermel, R.C. (1991). Predicting behavior and size of crown fires in the northern Rocky Mountains. USDA For. Serv. Res. Pap. INT-438.
41. Rothermel, R.C. (1998). Long range fire assessments. In K. Close & R.A. Bartlette (Eds.) Proc. Of the Interior West Fire Council Meeting and Symposium Coeur d'Alene, ID, November 1–3 1994, Intl. Asso. of Wildl. Fire, Fairfield, WA, pp 169–180.
42. Schroeder, M. J., & Buck, C. C. (1970). *Fire weather: A guide for application of meteorological information to forest fire control operations*. Agricultural Handbook: USDA. 360.
43. Scott, J.H. (2006). An analytical framework for quantifying wildland fire risk and fuel treatment benefit. In: P.L. Andrews & B.W. Butler (compilers) Fuel management—How to measure success: Conference Proceedings, 28–30 March, Portland OR, USDA For. Serv. Gen. Tech. Rep. RMRS-P-41, pp. 169–184.
44. Scott, J.H. & Burgan, R. (2005). Standard fire behavior fuel models: A comprehensive set for use with Rothermel's surface fire spread model. USDA Forest Service, Rocky Mountain Research Station, General Technical Report RMRS-GTR-153
45. Silvillo, J. K., Ahlquist, J. E., & Toth, Z. (1997). An ensemble forecasting primer. *Weather Forecasting, 12*(4), 809–818.
46. Toth, Z., & Kalnay, E. (1997). Ensemble forecasting at NCEP and the breeding method. *Monthly Weather Review, 125*, 3297–3319.
47. Van Wagner, C. E. (1977). Conditions for the start and spread of crown fire. *Canadian Journal of Forest Research, 7*, 23–34.
48. Wiitala, M.R. & Carlton, D.W. (1994). Assessing long-term fire movement risk in wilderness fire management. In Proc. 12th conference on Fire Forest Meteorology, Oct. 26–28, Jekyll Island Georgia, Soc. Am. Foresters, Bethesda, MD.